(Received 13 August 2025, Accepted 22 October 2025, Scheduled 7 November 2025)

Compact UWB MIMO Antenna with Minangkabau Roof-Inspired Patch and L-Shaped Ground Strip for Enhanced Bandwidth

Firdaus Firdaus[1,2], Rahmadi Kurnia[1], and Ikhwana Elfitri[1,*]

[1] *Department of Electrical Engineering, Universitas Andalas, Padang, Indonesia*
[2] *Department of Electrical Engineering, Politeknik Negeri Padang, Padang, Indonesia*

ABSTRACT: A compact ultra-wideband (UWB) multiple-input multiple-output (MIMO) antenna with a culturally inspired radiating structure is developed in this study. The radiating element is inspired by the traditional *gonjong* shape of Minangkabau architecture, which resembles upward-curving buffalo horns, forming a distinctive roof-like patch that enhances the impedance characteristics. A 50-ohm microstrip line is used to excite the patch, with a partial ground plane placed beneath the patch. To improve bandwidth and support low-frequency operation, an L-shaped strip is introduced on the ground plane, and the patch is optimized through edge modification and parametric analysis. The antenna achieves a wide measured impedance bandwidth of 2.2–20 GHz ($S_{11} < -10$ dB), fully covering and extending beyond the Federal Communications Commission (FCC)-defined UWB range. High isolation is achieved with S_{12} consistently below -20 dB across the band. Excellent MIMO performance is demonstrated with an envelope correlation coefficient (ECC) below 0.01, diversity gain (DG) above 9.95 dB, channel capacity loss (CCL) lower than 0.4 bit/s/Hz, and Total Active Reflection Coefficient (TARC) below -10 dB. The antenna also exhibits stable radiation patterns and maintains high efficiency throughout the operating band. With overall dimensions of just 30×30 mm^2, the developed antenna is more compact than most recent UWB MIMO designs, making it highly suitable for modern wireless communication systems requiring wide bandwidth and reliable multi-antenna performance.

1. INTRODUCTION

In recent years, the rapid growth of wireless communication services has been accompanied by an increasing demand for higher data transfer rates, driven by applications such as ultra-high definition video streaming [1], virtual and augmented reality in real time, and the low-latency industrial Internet of Things (IoT) [2]. Technologies such as 5G, Wi-Fi 6, and WiGig have been developed to support data rates in the gigabit per second (Gbit/s) range, enabling faster and more efficient wireless communication [3]. However, achieving such high data rates while maintaining low power consumption, high reliability, and compact device size remains a significant challenge. To address this, the integration of Ultrawideband (UWB) and Multiple Input Multiple Output (MIMO) technologies has emerged as a promising solution, offering high spectral efficiency, spatial diversity, and the potential to support wireless communication systems with data rates up to 1 Gbit/s [4, 5].

Effective antenna design is essential for unlocking the capabilities of UWB-MIMO systems, as it must support wideband operation within the FCC-allocated UWB range (3.1–10.6 GHz [6]), while ensuring high isolation, low mutual coupling, and compact dimensions to accommodate multiple elements within a limited area. These requirements are particularly challenging due to the trade-offs among bandwidth, efficiency, radiation characteristics, and physical size. Furthermore, the antenna design has a direct impact on the overall system performance, influencing factors such as signal quality, spatial diversity, and interference mitigation. Therefore, an effective UWB-MIMO antenna design is essential to realizing high data rates, robust wireless links, and reliable communication in modern high-speed wireless systems.

Various design strategies have been developed to address the challenges of implementing UWB-MIMO antennas, particularly in achieving wideband impedance matching, high inter-element isolation, and compact size. Techniques such as defected ground structures (DGSs), neutralization lines [7, 8], electromagnetic bandgap (EBG) structures [9, 10], orthogonal [11–13] or decoupling stubs [14–17], and parasitic decoupling structures [18] have been widely explored to reduce mutual coupling and improve isolation between closely spaced antenna elements. In addition, planar monopole and printed patch-based geometries [14, 17, 19–21] are often favored due to their simplicity, low profile, and ease of integration with compact devices. Recent studies have demonstrated innovative approaches such as incorporating L-shaped decoupling structures [22], parasitic elements [23], and ground slot modifications [24] to improve performance. Furthermore, antenna miniaturization can be achieved through shared radiator [25–28] and shared slot designs [29–31], which allow multiple elements to utilize common structures without significantly compromising performance. These advancements have contributed to the development of high-efficiency UWB-MIMO antennas suitable for contemporary wireless technologies such as 5G, short-range radar, and high-speed indoor communications.

Despite the significant progress in UWB-MIMO antenna research, many existing designs still face limitations in terms of

* Corresponding author: Ikhwana Elfitri (ikhwana@eng.unand.ac.id).

physical size, complexity, or insufficient isolation at close element spacing. As portable and embedded wireless systems continue to demand more compact and efficient components, there remains a need for UWB-MIMO antenna designs that offer a better balance among miniaturization, bandwidth performance, and inter-element decoupling. In this work, a novel 4×4 UWB-MIMO antenna is developed to effectively address these challenges. The antenna is designed with an overall size of only $30 \times 30\,\text{mm}^2$, making it more compact than many designs reported in the literature. It employs orthogonally arranged *gonjong*-shaped patch elements to enhance spatial diversity, while L-shaped decoupling structures are introduced between elements to improve impedance bandwidth and effectively suppress mutual coupling. To ensure practicality and affordability, the antenna is realized on an FR-4 substrate with 1.6 mm thickness and 4.4 dielectric constant. This compact and structurally simple configuration demonstrates strong potential for integration in space-constrained wireless devices without compromising communication performance.

2. ANTENNA DESIGN

2.1. UWB Antenna Element

Figure 1 shows the design structure of the developed UWB antenna, and the corresponding dimensional parameters are detailed in Table 1. The antenna features a compact structure with a patch inspired by the traditional *gonjong* roof shape, which reflects the architectural style of *rumah gadang*, a culturally significant Minangkabau house known for its pointed, buffalo-horn-like roof, commonly found in West Sumatra, Indonesia. A microstrip line implemented on a planar dielectric substrate serves as the excitation mechanism. A stepped structure is introduced between the feed line and roof-shaped patch, serving as an impedance matching section to support wideband performance. To improve the radiation characteristics, a partial ground plane is implemented on the backside of the substrate. Additionally, the impedance bandwidth is improved by integrating an L-shaped strip, particularly enhancing performance in the lower frequency region of UWB spectrum. This design ensures effective operation across the entire UWB and into higher frequencies, providing better impedance matching and stable radiation characteristics.

TABLE 1. Dimensions of optimized parameters of UWB antenna.

Parameters	a	b	c	d	e	f
Dimensions (mm)	5.77	10	3	2.72	2.2	1.25
Parameters	g	h	i	j	k	l
Dimensions (mm)	4.56	1	12	3	15	15

The progressive development of the antenna design, illustrated in Fig. 2, is guided by the simulated reflection coefficient (S_{11}) response. A structured six-stage procedure is employed to optimize the antenna's UWB performance.

In Step 1, the initial antenna design consists of a standard rectangular microstrip patch, whose dimensions are calculated using classical patch antenna equations with a center frequency

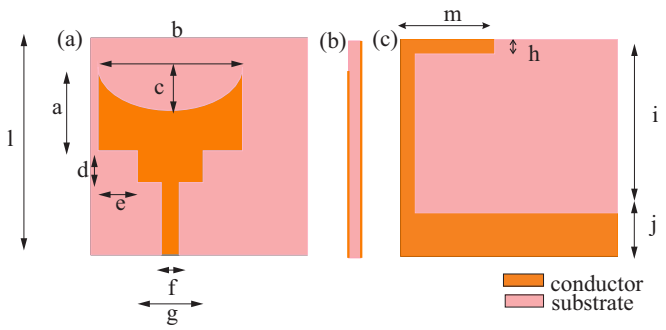

FIGURE 1. UWB antenna design, (a) front view, (b) side view, (c) back view.

of 8 GHz — corresponding to the midpoint of the UWB range. Although this configuration generates a sharp resonance at approximately 8.33 GHz with $S_{11} = -28.89$ dB, the impedance bandwidth is very narrow and does not satisfy the requirements of UWB operation. Therefore, further modifications are carried out in the next design steps to enhance bandwidth and achieve the desired UWB characteristics.

In Step 2, a horizontal step is added between the feed line and the patch, improving impedance matching with respect to the -10 dB S_{11} threshold. This modification expands the bandwidth significantly, covering approximately 4.39 GHz to 12.29 GHz. However, the achieved range is still insufficient to fully satisfy the UWB requirement.

In Step 3, the patch is further modified by adding a semicircular top, forming the basis of the gonjong shape inspired by Minangkabau architecture. This geometrical refinement broadens the impedance bandwidth, extending coverage from around 4.40 GHz to 13.68 GHz.

Step 4 introduces a stepped structure between the feedline and the patch, effectively increasing the electrical length. This adjustment enhances impedance matching, particularly in the mid-frequency range, and results in wider bandwidth as defined by the -10 dB S_{11} criterion.

In Step 5, a vertical strip is placed on the backside and directly connected to the partial ground plane. This element improves current flow and contributes to better matching in the mid-to-lower UWB region, resulting in bandwidth expansion from approximately 4.27 GHz to 16.3 GHz.

Finally, in Step 6, a horizontal strip is added and connected to the vertical one, forming an inverted L-shaped structure. This last enhancement strengthens performance at the lower end of the UWB and smooths the overall S_{11} response. The finalized antenna exhibits consistent performance across a wide range, maintaining S_{11} below -10 dB throughout 3.05 GHz to 16.3 GHz.

Parametric studies are essential in UWB antenna design, as they provide a deeper understanding of how each structural parameter influences the overall antenna performance. In this work, the variation in the reflection coefficient (S_{11}) is observed with respect to changes in several geometric parameters, including the depth of the patch notch (c), the corner cuts on the bottom of the patch (d, e), and the dimensions of the L-shaped strips added to the ground plane. The simulation results are illustrated in Fig. 3(a) to Fig. 3(h).

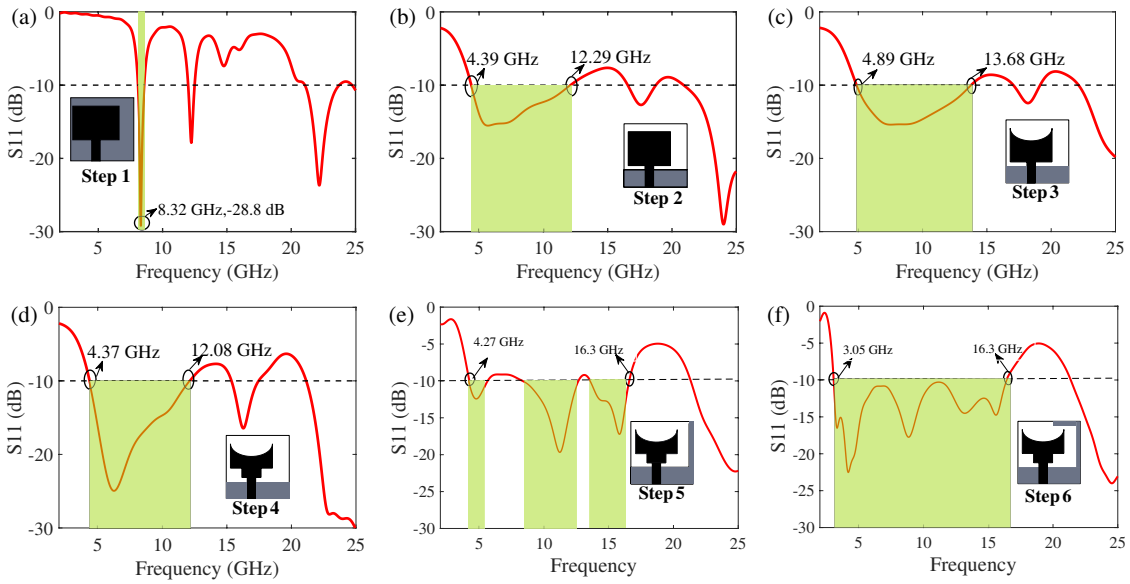

FIGURE 2. Reflection coefficient (S_{11}) performance at each design step of the developed UWB antenna. (a) Step 1, (b) step 2, (c) step 3, (d) step 4, (e) step 5, and (f) step 6.

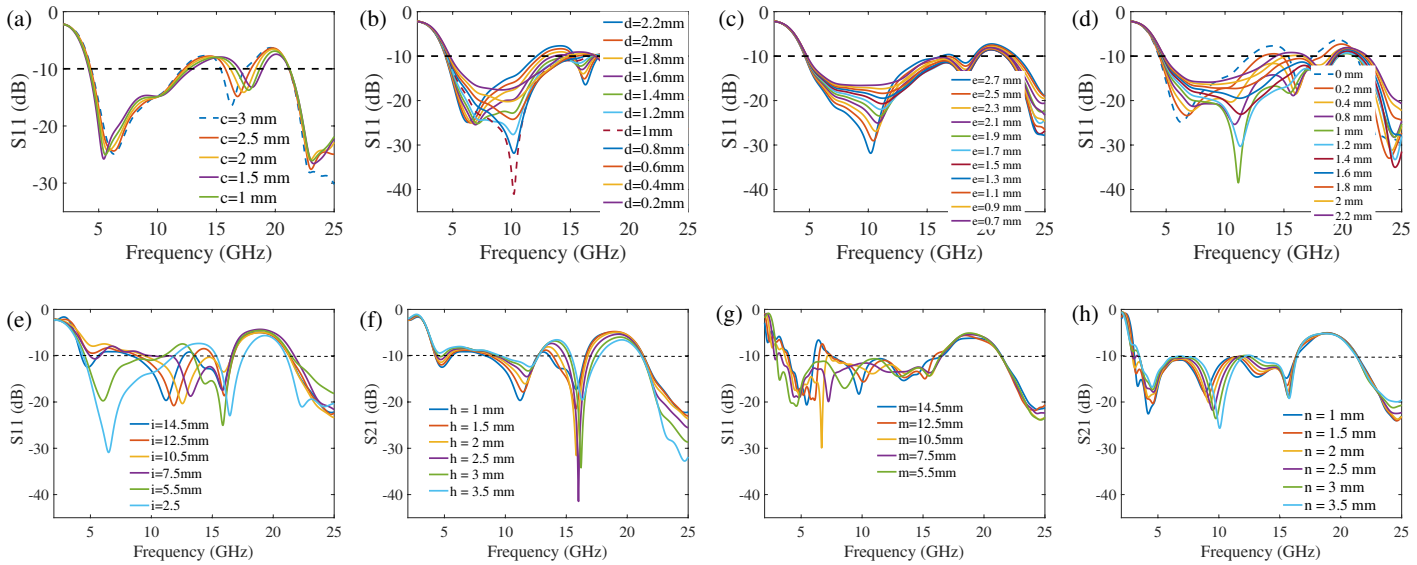

FIGURE 3. Parametric study of the UWB antenna design showing the impact of geometric parameters on the reflection coefficient (S_{11}): (a) variation of c, (b) variation of d, (c) variation of e, (d) combined variation of d and e, (e) variation of vertical strip length i, (f) variation of vertical strip width n, (g) variation of horizontal strip length m, (h) horizontal strip witdh n.

Figure 3(a) shows how changes in parameterc, defined as the center notch depth, impact the antenna's response, with values ranging from 0 to 2 mm. This parameter significantly influences the impedance bandwidth. As c increases, the bandwidth defined by the -10 dB S_{11} threshold becomes broader, indicating enhanced impedance matching over a wider frequency range. At certain values of c, the antenna achieves a consistently low reflection coefficient across the UWB, demonstrating optimal bandwidth performance.

Figure 3(b) presents the effect of varying parameter d, which defines the vertical depth of the corner cut at the bottom of the radiating patch. Smaller values of d lead to limited bandwidth, especially at lower frequencies. As d increases, the impedance bandwidth improves markedly, particularly within the 4–9 GHz range. An optimal value around 2.5 mm results in the broadest bandwidth, indicating effective enhancement of the antenna's matching characteristics.

The influence of parameter e is shown in Fig. 3(c). This parameter corresponds to the horizontal length of the bottom corner cut on the patch. After determining the optimal value of d, varying e further contributes to enhancing impedance bandwidth. The simulated S_{11} remains consistently below -10 dB over a broad frequency span, roughly between 4.5 GHz and 19.4 GHz, emphasizing the importance of parameter e in ensuring extensive UWB performance.

For further optimization, a simultaneous variation of parameters d and e with identical values is conducted, as depicted in Fig. 3(d). As a result of the combined parameter tuning, the an-

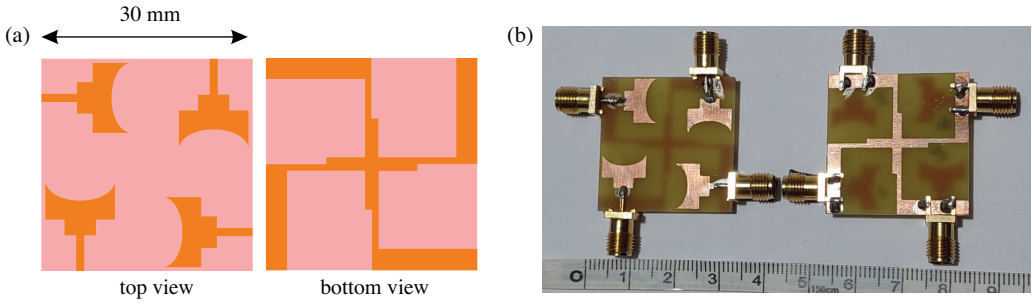

FIGURE 4. (a) Layout of the developed 4×4 UWB MIMO antenna. (b) Printed Antenna.

tenna achieves a highly stable and extensive impedance bandwidth, with S_{11} consistently remaining under -10 dB across the whole UWB spectrum. The optimal performance is obtained when $d = e = 2.5$ mm. Increasing both parameters beyond this value causes deterioration in matching near the band edges, suggesting the presence of an optimal configuration for achieving the best wideband behavior.

The effect of changing the vertical strip length (i) is illustrated in Fig. 3(e). The simulation results indicate that this parameter significantly influences the impedance bandwidth, particularly in the mid-frequency range (6–9 GHz). A moderate strip length provides the broadest bandwidth with S_{11} below -10 dB, while excessively short or long strips result in reduced bandwidth and degraded matching performance.

Figure 3(f) presents the impact of modifying the vertical strip width (b) on the antenna characteristics. This parameter plays a role in fine-tuning the impedance bandwidth across the UWB range. A well-balanced width value results in broader bandwidth and better matching, particularly in the mid-frequency region, while excessively narrow or wide strips reduce the overall -10 dB bandwidth performance.

The effect of the horizontal strip length (m) is illustrated in Fig. 3(g). Increasing m improves impedance matching at lower frequencies and extends the usable bandwidth within the 3–6 GHz range. However, if the strip is too long, the impedance performance deteriorates across the band due to detuning effects, indicating that an optimal length is necessary to maintain a broad and stable bandwidth.

The final parameter examined is the width of the horizontal strip (a), as shown in Fig. 3(h). Although its impact is less significant than the strip length, adjusting a can still enhance impedance matching at higher frequencies. Simulation results indicate that moderate increases in width lead to smoother S_{11} profiles and improved bandwidth coverage in the upper UWB region, particularly between 10 and 16 GHz.

The comprehensive analysis confirms that each geometric variation exerts a considerable influence on impedance matching and bandwidth performance. The findings demonstrate that precise adjustment of these parameters is essential for achieving optimal wideband behavior. By carefully combining the most favorable values identified in this analysis, the final antenna design achieves robust impedance matching across the entire 3.05–16.39 GHz range, ensuring efficient and reliable operation throughout the UWB spectrum.

2.2. MIMO Antenna Configuration

The optimized UWB antenna is further extended into a compact 4×4 MIMO configuration. Fig. 4(a) presents the structural design of the 4×4 UWB MIMO antenna which consists of individual elements, which retains the same compact size of 15×15 mm^2 as the single-element design, resulting in a total antenna dimension of 30×30 mm^2. The elements are arranged orthogonally and placed in close proximity, enabling improved isolation and polarization diversity.

To suppress mutual coupling, the L-shaped strip originally introduced to enhance impedance bandwidth in the single-element UWB design is repurposed as a decoupling structure placed between adjacent MIMO elements. The L-strips of each element are connected to each other, thereby linking the ground planes of all elements. This configuration not only ensures that the MIMO elements share a common ground plane, which is essential for practical implementation, but also helps achieve high isolation performance. This dual-function feature effectively suppresses surface current interactions while preserving wideband performance. The combination of orthogonal orientation and the decoupling strip significantly improves isolation and reduces the envelope correlation coefficient (ECC), thereby supporting robust MIMO operation.

3. RESULTS AND DISCUSSION

The printed UWB MIMO antenna, illustrated in Fig. 4(b), employs an FR4 substrate characterized by a thickness of 1.6 mm and a relative permittivity of 4.4. The simulated scattering parameters of the developed UWB MIMO antenna are depicted in Fig. 5. The S_{11} does not exceed -10 dB throughout the 2.6–20.6 GHz range, demonstrating excellent impedance matching and significantly broader bandwidth than the standard FCC-defined UWB spectrum (3.1–10.6 GHz). This wide operating range enhances the antenna's versatility for various high-frequency applications beyond conventional UWB systems.

In terms of mutual coupling, the transmission coefficients such as S_{21}, S_{31}, and S_{41} remain below -20 dB across most of the frequency band, indicating strong isolation between antenna elements. Such isolation is essential in MIMO configurations to reduce channel correlation and improve spatial diversity performance.

The measurement of the scattering parameters for the printed UWB MIMO antenna is presented in Fig. 6. As observed, the measured reflection coefficient (S_{11}) remains below -10 dB

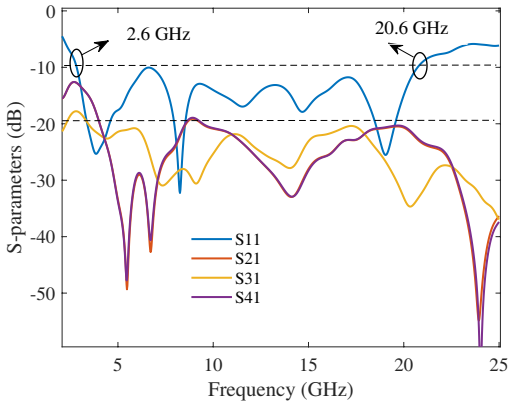

FIGURE 5. Simulated S-parameters of the developed UWB MIMO antenna.

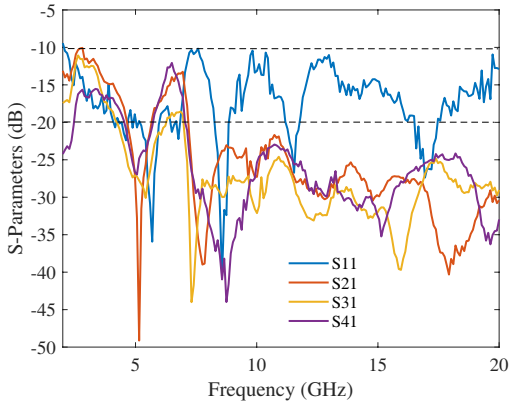

FIGURE 6. Measured scattering parameters of the UWB MIMO antenna.

from approximately 2.1 GHz to 20 GHz, closely matching the simulated bandwidth. This confirms that the fabricated antenna maintains stable impedance characteristics across a broad frequency band, despite slight deviations from the simulated result due to fabrication tolerances, connector losses, and measurement uncertainties. Nevertheless, the antenna successfully covers the FCC-defined UWB range (3.1–10.6 GHz) and, based on simulation results, achieves a wide operating bandwidth from 2.6 to 20.6 GHz, highlighting its potential for extended high-frequency applications.

Regarding mutual coupling, the measured transmission coefficients (S_{21}, S_{31}, and S_{41}) generally remain below -18 dB across most of the operating band, validating the strong isolation predicted in simulation. Although some variation exists compared to the simulated isolation levels (which were mostly below -20 dB), the overall performance still satisfies the isolation requirements for effective MIMO operation. This low mutual coupling ensures reduced inter-element interference and improved spatial diversity, enabling the antenna to perform effectively in dependable UWB MIMO communication systems.

To further validate the antenna's performance, a detailed comparison between the simulated and measured S_{11} and S_{12} parameters is presented in Fig. 7. As observed, the measured reflection coefficient (S_{11}) closely follows the simulated result, remaining under -10 dB throughout the majority of the UWB

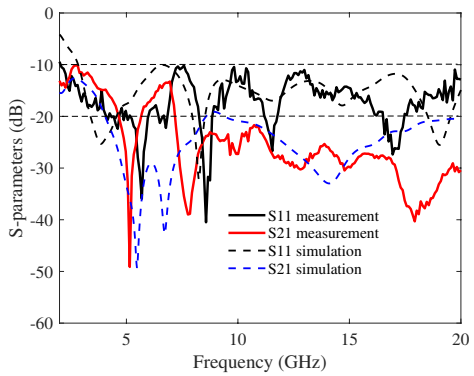

FIGURE 7. S-parameter comparison (S_{11} and S_{12}) between simulation and measurement.

spectrum. Minor discrepancies, particularly at the band edges, can be attributed to fabrication imperfections, substrate losses, and connector mismatches.

Similarly, the transmission coefficient (S_{12}), which indicates the level of mutual coupling between adjacent antenna elements, shows good agreement between simulation and measurement. Both results remain below -18 dB over a wide frequency range, confirming the impact of the integrated decoupling structure and orthogonal element placement in suppressing mutual coupling. The consistent performance in both simulation and measurement affirms the robustness and practical feasibility of the developed MIMO antenna for UWB applications.

The effect of element spacing on the proposed UWB MIMO antenna was investigated by symmetrically shifting the antenna elements away from the substrate center, with the separation varied from 0 to 2.5 mm in steps of 0.5 mm. This variation, illustrated in Fig. 8, is represented by the legend s, which denotes the element shifting. The reflection coefficient (S_{11}) remains relatively stable across most of the band. However, in some cases, portions of the response exceed -10 dB. This indicates degraded impedance matching and a reduction of the effective UWB bandwidth. The transmission coefficient (S_{21}) shows greater sensitivity to spacing. Larger separations generally improve isolation, particularly below 10 GHz. These results highlight a trade-off between impedance bandwidth and isolation. An element spacing of 1.5–2.0 mm offers an optimal balance between compact size, wideband matching, and reduced mutual coupling.

The gain performance of the developed UWB MIMO antenna, based on both simulation and measurement, is shown in Fig. 9. Overall, the gain remains relatively stable across the ultra-wideband range. The simulated gain varies between approximately 1.2 and 4 dBi, while the measured results show a comparable trend, ranging from about 1.2 to 2.2 dBi. In addition to gain, Fig. 9 also presents the radiation efficiency and the total efficiency of the antenna. The simulated radiation efficiency, depicted by the solid blue line, indicates that the antenna maintains a reasonable radiation capability over the entire frequency band, with values mostly above -4 dB. Meanwhile,

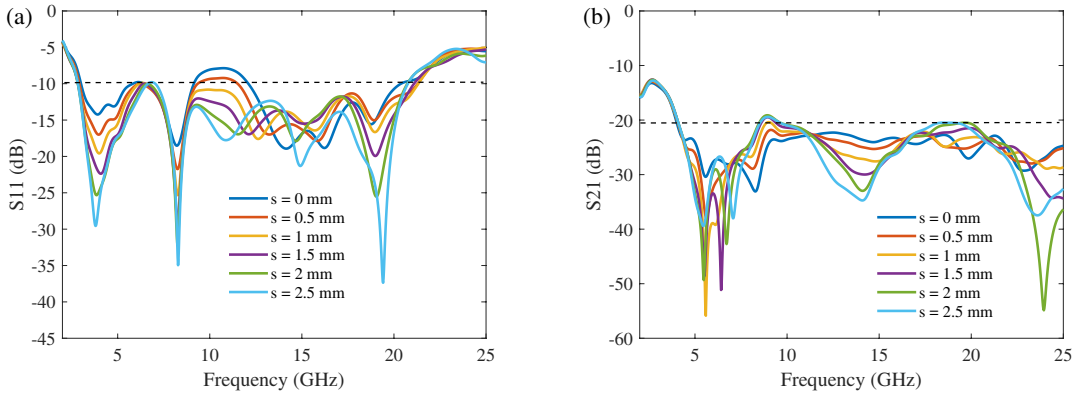

FIGURE 8. Simulated S-parameters of the proposed UWB MIMO antenna for different element spacing variations, where the center patch is shifted from 0 to 2.5 mm with 0.5 mm step. (a) Reflection coefficient (S_{11}) and (b) transmission coefficient (S_{21}).

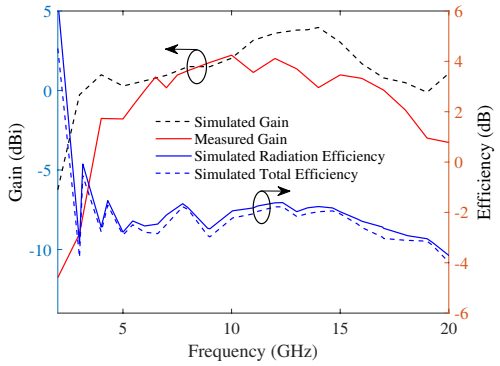

FIGURE 9. Gain and efficiency of the developed UWB MIMO antenna, including simulated and measured gain, simulated radiation efficiency, and simulated total efficiency.

the simulated total efficiency, represented by the blue triangular markers, follows a similar trend but with slightly reduced values due to the combined effects of radiation loss and impedance mismatch. These results demonstrate that the proposed UWB MIMO antenna not only provides stable gain but also achieves acceptable efficiency performance across the operating band.

To better understand the isolation mechanism and current distribution behavior, Fig. 10 presents the surface current distribution of the developed UWB MIMO antenna when Port 1 is excited at a representative frequency. As shown, strong current concentrations are observed around the excited element, while significantly weaker currents are induced on the adjacent elements. This indicates effective suppression of mutual coupling, largely attributed to the orthogonal placement of antenna elements and the presence of the central inverted L-shaped decoupling strip. The decoupling structure redirects surface currents away from neighboring elements, minimizing undesired coupling and supporting good isolation across the operating band.

To thoroughly evaluate MIMO characteristics of the designed 4×4 UWB MIMO antenna, four key metrics, namely Envelope Correlation Coefficient (ECC), Diversity Gain (DG), Channel Capacity Loss (CCL), and Total Active Reflection Coefficient (TARC), are investigated.

ECC measures the degree of coupling between antenna elements and is crucial for assessing spatial diversity. Ideally, ECC should be close to zero, indicating low correlation and high diversity performance. There are two common approaches to calculate ECC, namely using far-field radiation patterns of the antenna elements or using scattering parameters (S-parameters). In this work, ECC is estimated using S-parameters as [32]:

$$\mathrm{ECC} = \frac{\left|S_{ii}^{*}S_{ij} + S_{ji}^{*}S_{jj}\right|^{2}}{\left(1 - |S_{ii}|^{2} - |S_{ji}|^{2}\right)\left(1 - |S_{jj}|^{2} - |S_{ij}|^{2}\right)} \tag{1}$$

Diversity Gain (DG) indicates how much diversity is gained in signal reception and is related to ECC by:

$$\mathrm{DG} = 10\sqrt{1 - (\mathrm{ECC})^{2}} \tag{2}$$

Figure 11 presents both simulated and measured values of ECC and DG across the UWB. The ECC remains well below 0.01 for both simulation and measurement, indicating excellent spatial decorrelation and minimal mutual coupling. The DG values are also close to the theoretical maximum of 10 dB, confirming strong diversity performance. While the measured results generally follow the simulation trends, a slight degradation in DG is observed in the lower frequency range (3–4.5 GHz), likely due to increased loss or imperfect matching in the fabricated prototype. However, the overall consistency between simulation and measurement validates the robustness and effectiveness of the UWB MIMO antenna design developed.

CCL measures the decrease in channel capacity caused by mutual coupling and signal correlation. A low CCL indicates better channel utilization and improved throughput in multipath environments. CCL is computed from the determinant of the receiver correlation matrix Ψ^{R} as follows [33]:

$$C_{\mathrm{loss}} = -\log_{2}\left(\left|\Psi^{R}\right|\right) \tag{3}$$

where

$$\Psi^{R} = \begin{bmatrix} \rho_{11} & \rho_{12} & \rho_{13} & \rho_{14} \\ \rho_{21} & \rho_{22} & \rho_{23} & \rho_{24} \\ \rho_{31} & \rho_{32} & \rho_{33} & \rho_{34} \\ \rho_{41} & \rho_{42} & \rho_{43} & \rho_{44} \end{bmatrix} \tag{4}$$

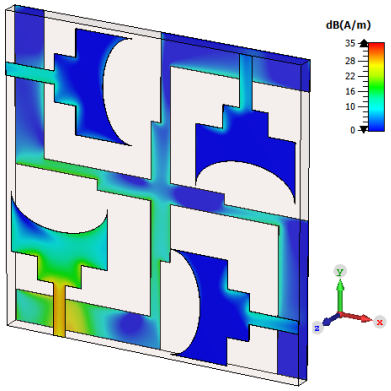

FIGURE 10. Surface current behavior at a representative frequency is analyzed through simulation when Port 1 of the developed UWB MIMO antenna is activated.

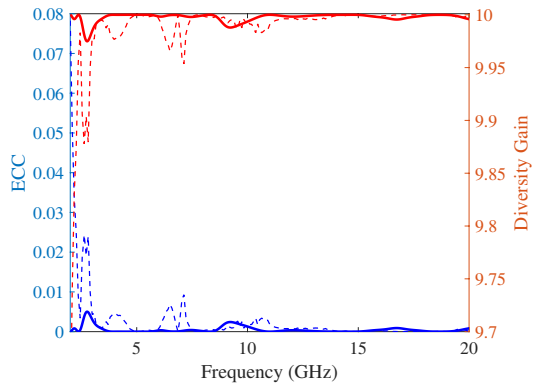

FIGURE 11. Simulated and measured envelope correlation coefficients (ECCs) and diversity gains (DGs).

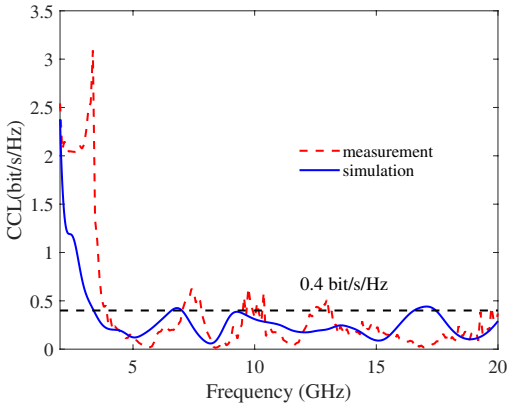

FIGURE 12. Simulated and measured Channel Capacity Losses (CCLs) of the developed UWB MIMO antenna.

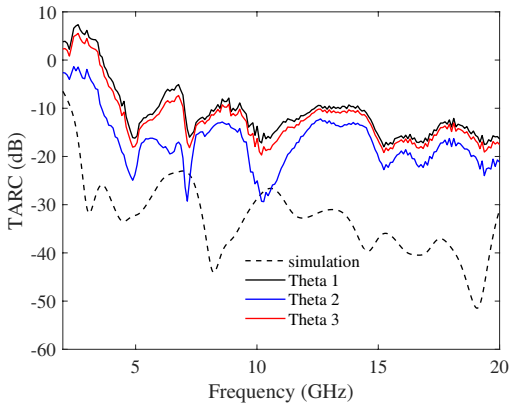

FIGURE 13. Simulated and measured Total Active Reflection Coefficients (TARCs) of the developed UWB MIMO antenna.

The correlation coefficients ρ_{ij} are derived from S-parameters as:

$$\rho_{ii} = 1 - \left| \sum_{n=1}^{4} S_{ni}^{*} S_{ni} \right| \tag{5}$$

$$\rho_{ij} = - \left| \sum_{n=1}^{4} S_{ni}^{*} S_{nj} \right|, \quad i \neq j \tag{6}$$

As shown in Fig. 12, the simulated CCL remains consistently below 0.35 bit/s/Hz across the UWB, indicating good isolation and minimal degradation in channel capacity. In contrast, the measured CCL exhibits higher values, with several frequency points — particularly in the lower part of the UWB band — exceeding the threshold of 0.4 bit/s/Hz. It suggests that the practical isolation performance is not as strong as predicted in simulation, especially at lower frequencies. Nevertheless, the CCL remains within acceptable limits for most of the band, supporting the viability of the antenna for UWB MIMO applications.

TARC evaluates the combined effect of mutual coupling and active port excitation. Unlike traditional reflection coefficients, TARC considers simultaneous excitations and is defined as [34, 35]:

$$\text{TARC} = \sqrt{\frac{\sum_{i=1}^{N} |b_i|^2}{\sum_{i=1}^{N} |a_i|^2}} \tag{7}$$

In this context, a_i and b_i represent the incident and reflected voltage waves at port i, respectively. These quantities are linked through the S-parameter matrix as:

$$\mathbf{b} = \mathbf{Sa} \tag{8}$$

By inserting Equations (7) and (8) into the formulation, the Total Active Reflection Coefficient (TARC) can be reformulated in terms of the S-parameters as follows:

$$\text{TARC} = \sqrt{\left| \sum_{i=1}^{4} S_{i1} + \sum_{n=2}^{4} S_{in} e^{j\theta_{n-1}} \right|^2 \Big/ 2} \tag{9}$$

where θ_i is the phase of the ith input signal.

The Total Active Reflection Coefficient (TARC) results, obtained through simulation and measurement, are presented in Fig. 13 for the developed UWB MIMO antenna. The simulated TARC is computed using a single constant-phase

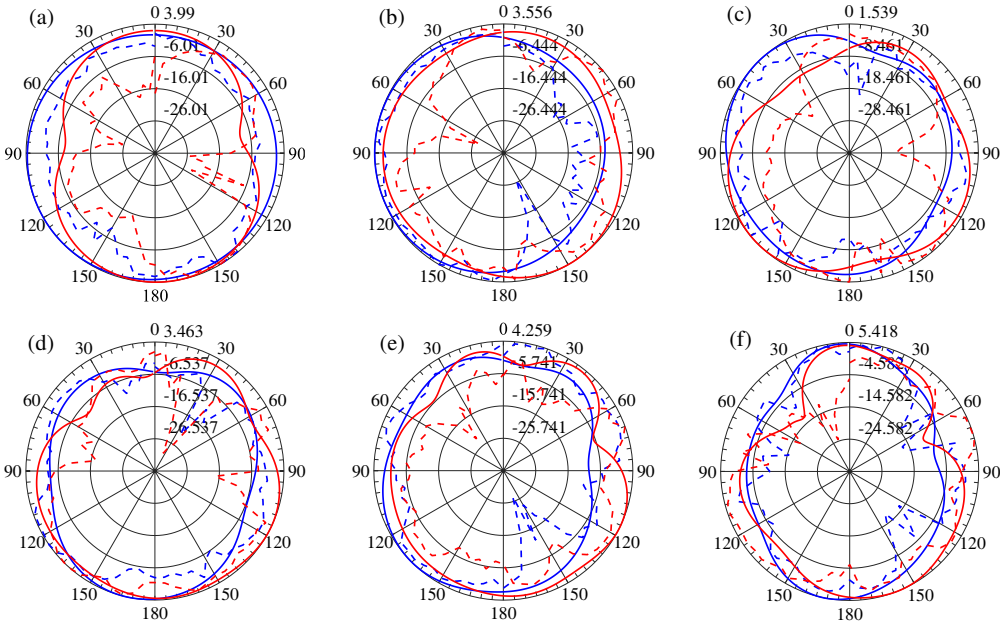

FIGURE 14. Radiation patterns of the proposed UWB MIMO antenna at discrete frequencies within the UWB spectrum (E-plane = blue, H-plane = red; solid = simulation, dashed = measurement). (a) 2 GHz, (b) 4 GHz, (c) 6 GHz, (d) 8 GHz, (e) 10 GHz, and (f) 12 GHz.

TABLE 2. Comparative summary of UWB MIMO antenna designs.

Ref.	Size (mm)	Ports	Bandwidth (GHz)	Isolation (dB)	ECC	Peak Gain (dBi)
[11]	39×39	4×4	2.3–11.7	< 22	0.025	4.7
[9]	38.3×38.3	4×4	3–13.2	< 17	0.02	6.6
[36]	34×34	4×4	3.1–10.6	4	0.025	4.03
[14]	45×45	4×4	2–10.6	-17	0.03	4.5
[35]	50×50	4×4	3.3–60	-30	0.00021	5
This work	30×30	4×4	2.2–20	< 20	< 0.01	3

excitation across all ports, whereas the measured TARC is derived from S-parameter data under three randomly selected phase excitation conditions to emulate realistic MIMO scenarios. The results show that the TARC remains below -10 dB across most of the 3.1–20 GHz range, indicating effective impedance matching and low reflection. Although simulated and measured curves follow a similar trend, the simulated TARC demonstrates slightly better performance, remaining consistently lower throughout the band. This improvement is expected due to the idealized conditions in simulation, which exclude the effects of fabrication tolerances, connector mismatches, and measurement setup imperfections. Nevertheless, the overall agreement between simulation and measurement results confirms the developed antenna's capability to maintain high radiation efficiency and low return loss in practical MIMO applications.

The E-plane (blue) and H-plane (red) radiation patterns of the developed UWB MIMO antenna at six representative frequencies (2, 4, 6, 8, 10, and 12 GHz) are shown in Fig. 14, including both simulated (solid) and measured (dashed) results for comparison. At lower frequencies (2–4 GHz), the antenna exhibits nearly omnidirectional radiation in both planes, which is desirable for achieving wide spatial coverage and diversity. As the frequency increases (6–12 GHz), the patterns become more directive with noticeable lobe formation, a behavior typical of compact UWB antennas due to higher-order mode excitations and ground-plane effects. Overall, good agreement between simulation and measurement validates the radiation performance across the UWB, with minor discrepancies observed at higher frequencies (8–12 GHz) where additional lobes and asymmetries appear. These differences are primarily attributed to environmental factors during measurement.

It should be noted that the radiation patterns were measured in an open outdoor environment rather than in an anechoic chamber. Consequently, reflections from surrounding objects and ground surfaces may have influenced the results, particularly at higher frequencies where the wavelength becomes comparable to the dimensions of nearby structures. Nevertheless, the measurements confirm the overall stability and performance of the proposed antenna design.

Table 2 presents a performance comparison between the developed antenna and several recent UWB MIMO antenna designs reported in the literature. With dimensions of $30 \times 30\,\text{mm}^2$, the developed antenna offers a more compact footprint than many existing designs, making it well-suited for integration into devices with limited space. Despite its compact dimensions, the antenna supports a wide operational bandwidth of 3.02–11.71 GHz, effectively covering the entire UWB range. In terms of mutual coupling, the design provides an isolation lower than $-20\,\text{dB}$ across the operating band, which is competitive with other reported antennas and sufficient for practical MIMO operation. The envelope correlation coefficient (ECC) is maintained below 0.01, indicating excellent diversity performance. Nevertheless, the maximum gain achieved by the developed antenna is observed at approximately 3 dBi, which is relatively lower than some other designs that achieve gains above 4 dBi. The relatively lower gain can be attributed to the compact physical dimensions and the design focus on improving bandwidth and isolation. Nevertheless, the antenna maintains a good balance among size, bandwidth, isolation, and diversity performance, which makes it a strong candidate for UWB MIMO applications where miniaturization and isolation are prioritized over high gain. Overall, the simulation and measurement results comprehensively demonstrate the effectiveness of the developed UWB MIMO antenna design. The parametric analysis confirms the critical role of geometric optimization in achieving wide impedance bandwidth and proper impedance matching. The extension to a compact 4×4 MIMO configuration successfully maintains performance while achieving good isolation and polarization diversity, aided by the incorporation of an inverted L-shaped decoupling structure. Although minor discrepancies are observed between simulation and measurement — particularly at lower frequencies — they are likely due to fabrication imperfections, connector mismatches, or environmental factors during open-area measurements.

4. CONCLUSION

A compact UWB MIMO antenna with broad bandwidth and strong isolation has been realized. Through a comprehensive parametric analysis, critical geometrical parameters were optimized to achieve wideband performance and improved impedance matching. The final design demonstrates a broad impedance bandwidth ranging from 2.2 to 20 GHz, effectively covering and exceeding the FCC-defined UWB range. The measured and simulated results show good agreement in terms of S-parameters, gain, and diversity performance metrics. The antenna exhibits a low envelope correlation coefficient (< 0.01), high diversity gain (near 10 dB), low channel capacity loss (below 0.4 bps/Hz), and a TARC below $-10\,\text{dB}$ across most of the UWB. These characteristics confirm the antenna's ability to operate efficiently in realistic MIMO environments with low mutual coupling and high radiation efficiency. The developed antenna is well-suited for emerging UWB applications including high-data-rate wireless communication, radar imaging, and short-range localization, where compact size, wide bandwidth, and robust MIMO performance are required.

REFERENCES

[1] He, J., J. Yuan, and F. Xing, "DVL2024: A larger ultra high definition video dataset for perceptual quality study," *IEEE Access*, Vol. 13, 40 429–40 437, 2025.

[2] Martalò, M., G. Pettorru, and L. Atzori, "A cross-layer survey on secure and low-latency communications in next-generation IoT," *IEEE Transactions on Network and Service Management*, Vol. 21, No. 4, 4669–4685, 2024.

[3] Mohamed, E. M., M. A. Abdelghany, and M. Zareei, "An efficient paradigm for multiband WiGig D2D networks," *IEEE Access*, Vol. 7, 70 032–70 045, 2019.

[4] Kaiser, T., F. Zheng, and E. Dimitrov, "An overview of ultra-wide-band systems with MIMO," *Proceedings of the IEEE*, Vol. 97, No. 2, 285–312, 2009.

[5] Bilal, M., R. Saleem, H. H. Abbasi, M. F. Shafique, and A. K. Brown, "An FSS-based nonplanar quad-element UWB-MIMO antenna system," *IEEE Antennas and Wireless Propagation Letters*, Vol. 16, 987–990, 2017.

[6] U.S. Federal Communications Commission (FCC), "Revision of part 15 of the commission's rules regarding ultra-wideband transmission systems, first report and order," ET Docket 98-153, FCC 02-48, 56 928–56 935, 2002.

[7] Kumari, P., R. K. Gangwar, and R. K. Chaudhary, "An aperture-coupled stepped dielectric resonator UWB MIMO antenna with AMC," *IEEE Antennas and Wireless Propagation Letters*, Vol. 21, No. 10, 2040–2044, 2022.

[8] Chaudhary, A. K. and M. Manohar, "A modified SWB hexagonal fractal spatial diversity antenna with high isolation using meander line approach," *IEEE Access*, Vol. 10, 10 238–10 250, 2022.

[9] Gómez-Villanueva, R. and H. Jardón-Aguilar, "Compact UWB uniplanar four-port MIMO antenna array with rejecting band," *IEEE Antennas and Wireless Propagation Letters*, Vol. 18, No. 12, 2543–2547, 2019.

[10] Wang, L., Z. Du, H. Yang, R. Ma, Y. Zhao, X. Cui, and X. Xi, "Compact UWB MIMO antenna with high isolation using fence-type decoupling structure," *IEEE Antennas and Wireless Propagation Letters*, Vol. 18, No. 8, 1641–1645, 2019.

[11] Tang, Z., X. Wu, J. Zhan, S. Hu, Z. Xi, and Y. Liu, "Compact UWB-MIMO antenna with high isolation and triple band-notched characteristics," *IEEE Access*, Vol. 7, 19 856–19 865, 2019.

[12] Yu, C., S. Yang, Y. Chen, W. Wang, L. Zhang, B. Li, and L. Wang, "A super-wideband and high isolation MIMO antenna system using a windmill-shaped decoupling structure," *IEEE Access*, Vol. 8, 115 767–115 777, 2020.

[13] Jayant, S. and G. Srivastava, "Close-packed quad-element triple-band-notched UWB MIMO antenna with upgrading capability," *IEEE Transactions on Antennas and Propagation*, Vol. 71, No. 1, 353–360, 2023.

[14] Tripathi, S., A. Mohan, and S. Yadav, "A compact Koch fractal UWB MIMO antenna with WLAN band-rejection," *IEEE Antennas and Wireless Propagation Letters*, Vol. 14, 1565–1568, 2015.

[15] Chandel, R., A. K. Gautam, and K. Rambabu, "Tapered fed compact UWB MIMO-diversity antenna with dual band-notched characteristics," *IEEE Transactions on Antennas and Propagation*, Vol. 66, No. 4, 1677–1684, 2018.

[16] Liu, L., S. W. Cheung, and T. I. Yuk, "Compact MIMO antenna for portable UWB applications with band-notched characteristic," *IEEE Transactions on Antennas and Propagation*, Vol. 63, No. 5, 1917–1924, 2015.

[17] Khan, M. S., A.-D. Capobianco, S. M. Asif, D. E. Anagnostou, R. M. Shubair, and B. D. Braaten, "A compact CSRR-enabled UWB diversity antenna," *IEEE Antennas and Wireless Propagation Letters*, Vol. 16, 808–812, 2017.

[18] Yao, Y., Y. Shao, J. Zhang, and J. Zhang, "A transparent antenna using metal mesh for UWB MIMO applications," *IEEE Transactions on Antennas and Propagation*, Vol. 71, No. 5, 3836–3844, May 2023.

[19] Desai, A., J. Kulkarni, M. M. Kamruzzaman, S. Hubálovský, H.-T. Hsu, and A. A. Ibrahim, "Interconnected CPW fed flexible 4-port MIMO antenna for UWB, X, and Ku band applications," *IEEE Access*, Vol. 10, 57 641–57 654, 2022.

[20] Rekha, V. S. D., P. Pardhasaradhi, B. T. P. Madhav, and Y. U. Devi, "Dual band notched orthogonal 4-element MIMO antenna with isolation for UWB applications," *IEEE Access*, Vol. 8, 145 871–145 880, 2020.

[21] Kumar, P., S. Urooj, and A. Malibari, "Design and implementation of quad-element super-wideband MIMO antenna for IoT applications," *IEEE Access*, Vol. 8, 226 697–226 704, 2020.

[22] Iqbal, A., O. A. Saraereh, A. W. Ahmad, and S. Bashir, "Mutual coupling reduction using F-shaped stubs in UWB-MIMO antenna," *IEEE Access*, Vol. 6, 2755–2759, 2018.

[23] Chen, Z., W. Zhou, and J. Hong, "A miniaturized MIMO antenna with triple band-notched characteristics for UWB applications," *IEEE Access*, Vol. 9, 63 646–63 655, 2021.

[24] Chattha, H. T., F. Latif, F. A. Tahir, M. U. Khan, and X. Yang, "Small-sized UWB MIMO antenna with band rejection capability," *IEEE Access*, Vol. 7, 121 816–121 824, 2019.

[25] MoradiKordalivand, A., T. A. Rahman, and M. Khalily, "Common elements wideband MIMO antenna system for WiFi/LTE access-point applications," *IEEE Antennas and Wireless Propagation Letters*, Vol. 13, 1601–1604, 2014.

[26] Mao, C.-X. and Q.-X. Chu, "Compact coradiator UWB-MIMO antenna with dual polarization," *IEEE Transactions on Antennas and Propagation*, Vol. 62, No. 9, 4474–4480, Sep. 2014.

[27] Hussain, R., M. S. Sharawi, and A. Shamim, "An integrated four-element slot-based MIMO and a UWB sensing antenna system for CR platforms," *IEEE Transactions on Antennas and Propagation*, Vol. 66, No. 2, 978–983, Feb. 2018.

[28] Kobal, E., R.-J. Liu, C. Yu, and A. Zhu, "A high isolation, low-profile, triple-port SIW based annular slot antenna for millimeter-wave 5G MIMO applications," *IEEE Access*, Vol. 10, 89 458–89 464, 2022.

[29] Gao, P., S. He, X. Wei, Z. Xu, N. Wang, and Y. Zheng, "Compact printed UWB diversity slot antenna with 5.5-GHz band-notched characteristics," *IEEE Antennas and Wireless Propagation Letters*, Vol. 13, 376–379, 2014.

[30] Kang, L., H. Li, X. Wang, and X. Shi, "Compact offset microstrip-fed MIMO antenna for band-notched UWB applications," *IEEE Antennas and Wireless Propagation Letters*, Vol. 14, 1754–1757, 2015.

[31] Saxena, S., B. K. Kanaujia, S. Dwari, S. Kumar, and R. Tiwari, "A compact dual-polarized MIMO antenna with distinct diversity performance for UWB applications," *IEEE Antennas and Wireless Propagation Letters*, Vol. 16, 3096–3099, 2017.

[32] Douhi, S., S. Mazroui, Z. Zakaria, S. Das, and A. Eddiai, "A 4-Port MIMO Antenna featuring multi-band functionality with improved isolation for terahertz systems," *IEEE Access*, Vol. 13, 132 223–132 236, 2025.

[33] Srivastava, G., S. Kumar, S. Alshathri, W. El-Shafai, and O. P. Kumar, "Compact UWB MIMO antenna with a modified back reflector and supported by characteristic mode analysis for wireless communication applications," *IEEE Access*, Vol. 12, 187 302–187 312, 2024.

[34] Manteghi, M. and Y. Rahmat-Samii, "Multiport characteristics of a wide-band cavity backed annular patch antenna for multipolarization operations," *IEEE Transactions on Antennas and Propagation*, Vol. 53, No. 1, 466–474, Jan. 2005.

[35] Elsharkawy, R. R., A. S. A. El-Hameed, and S. M. El-Nady, "Quad-port MIMO filtenna with high isolation employing BPF with high out-of-band rejection," *IEEE Access*, Vol. 10, 3814–3824, 2022.

[36] Shome, P. P., T. Khan, A. A. Kishk, and Y. M. M. Antar, "Quad-element MIMO antenna system using half-cut miniaturized UWB antenna for IoT-based smart home digital entertainment network," *IEEE Internet of Things Journal*, Vol. 10, No. 20, 17 964–17 976, 2023.